An Overview of the Visible and Infrared Scanner Radiometric Calibration Algorithm

ROBERT A. BARNES

General Sciences Corporation, Beltsville, Maryland

WILLIAM L. BARNES

Laboratory for Hydrospheric Processes, National Aeronautics and Space Administration, Goddard Space Flight Center, Greenbelt, Maryland

CHENG-HSUAN LYU

Caelum Research Corporation, Greenbelt, Maryland

JOEL M. GALES

George Mason University, Fairfax, Virginia

(Manuscript received 4 January 1999, in final form 17 May 1999)

ABSTRACT

The Visible and Infrared Scanner (VIRS) is one of the principal instruments on board the Tropical Rainfall Measuring Mission (TRMM) satellite. VIRS measurements provide cloud-top temperatures and structures that complement the rainfall rates derived from other TRMM sensors. The VIRS radiometric calibration algorithm converts the digital data downlinked from the instrument into spectral radiances. VIRS has five bands: one in the visible, one in the shortwave infrared, and three in the thermal infrared. The calibration algorithm treats each band in the same manner except that the visible and shortwave infrared bands do not respond to the thermal radiation emitted by the instrument, and these bands do not have the nonlinear responses with input radiance found in the thermal bands. The calibration coefficients for the visible and shortwave infrared bands were determined in the laboratory before launch. VIRS carries a reference blackbody that is used to update the calibration coefficients for the thermal bands for each scan of the instrument on orbit. In addition, VIRS uses an onboard diffuser to view the Sun approximately once per month. The VIRS radiometric algorithm uses measurements of these reference sources to provide calibrated spectral radiances for each Earth pixel that it views.

1. Introduction

The Visible and Infrared Scanner (VIRS) is one of the principal instruments onboard the Tropical Rainfall Measuring Mission (TRMM) satellite (Simpson et al. 1988). TRMM is a joint mission between the National Aeronautics and Space Administration (NASA) of the United States and the National Space Development Agency (NASDA) of Japan. The TRMM mission has been designed to measure rainfall and the exchange of energy—that is, the exchange of the latent heat of condensation—in the tropical and subtropical regions of the world. The atmosphere obtains three-fourths of its heat energy from the release of latent heat by precipitation, and it is estimated that two-thirds of the world's precipitation occurs in the Tropics. There has been a scarcity of quantitative precipitation information on a global basis. This is true particularly in the tropical regions, where 75% of the surface is covered by water. TRMM is now providing a regular long-term set of precipitation measurements in the Tropics and subtropics.

VIRS was not designed to measure rainfall. Onboard TRMM those measurements are made by the Precipitation Radar (PR) and the TRMM Microwave Imager (TMI). VIRS adds cloud-top temperatures and structures that complement the measurements from these microwave sensors. The connection between precipitation rates and cloud-top temperatures derived from TRMM should improve estimates of tropical precipitation rates using data from visible and infrared satellite instruments in the eras both before and after the TRMM mission.

The VIRS measurements in the visible and infrared

Corresponding author address: Dr. William L. Barnes, Laboratory for Hydrospheric Processes, NASA/GSFC, Code 970, Greenbelt, MD 20771.
E-mail: wbarnes@neptune.gsfc.nasa.gov

are similar to those on the Geostationary Operational Satellite (GOES) imagers (Pease 1991; Weinreb et al. 1997) and the Advanced Very High Resolution Radiometer (AVHRR) (Cracknell 1997). The center wavelengths and bandwidths for the five VIRS bands duplicate closely those on the GOES instruments. For the Moderate Resolution Imaging Spectroradiometer (MODIS) to be launched on the Earth Observing System (EOS) AM-1 and PM-1 platforms the similarity is even closer. VIRS is a simplified five-band version of MODIS. It has the same basic design as MODIS (Barnes et al. 1998), including components such as the scan mirror and the interference filters. The VIRS calibration algorithm accounts for many instrument characteristics that are similar to those of MODIS (Guenther et al. 1998) and the GOES imagers. An accurate calibration of the VIRS radiances is fundamental to their comparison with radiances from past, current, and future Earth imagers. In addition, these comparisons are fundamental to estimates of tropical precipitation both before and after the TRMM mission.

2. Instrument description

The VIRS radiometer (Barnes et al. 1996; Kummerow et al. 1998) was manufactured by Hughes Santa Barbara Remote Sensing (SBRS), now Raytheon Santa Barbara Research Center. VIRS uses a continuously rotating double-sided silver-coated scan mirror to reflect the radiance from the Earth and calibration targets into the scanner's Cassegrain telescope. This energy passes into a cooled focal plane with five detectors. The visible band (0.6 μm) uses a silicon photodiode. The shortwave infrared (SWIR; 1.6 μm) and midwave infrared (3.8 μm) bands use photovoltaic mercury cadmium telluride (HgCdTe) detectors, and the longwave infrared bands (10.8 and 11.9 μm) use photoconductive HgCdTe. For the discussions that follow, the midwave and longwave infrared bands are given the common title of ''thermal bands.'' The VIRS electronics convert the outputs from the detectors into digital numbers (DNs) for transmission to the ground.

As shown in Fig. 1, the Cassegrain telescope views the scan mirror with the axis of rotation of the mirror oriented perpendicular to the optical axis of the telescope. The telescope does not view the Earth or the calibration targets directly. For this reason, the VIRS instrument can be viewed as having four basic parts: the scan mirror, the radiometer (that is, the telescope and focal plane), the electronics module, and the calibration targets. The calibration targets include an onboard blackbody, an onboard solar diffuser, and a view of deep space.

The use of a paddle wheel mirror allows both sides of the mirror to scan both the Earth and the instrument's calibration targets during each revolution of the mirror. The incidence angles for the images viewed by the mirror are defined relative to the angle at which the mirror surface is normal to the optical axis of the telescope. This is the autoreflection angle. The timing of the Earth measurements is such that there are 261 samples of the Earth for each scan, and each Earth scan subtends an angle of 90°. Pixel 131 is the nadir sample, with pixels 1 and 261 at $\pm 45°$ from nadir. The positions of the calibration targets are such that they have incidence angles that are the same as those of portions of the Earth scan. As a result, the angles for the center of the space view and for the start of the Earth scan are numerically the same, and the two measurements are symmetrical with respect to the autoreflection angle.

3. Band-averaged spectral radiances

As shown in Fig. 2, the five VIRS bands have finite spectral bandwidths. That is, they do not measure at single wavelengths. In this figure, the spectral response for each band is normalized to a value of unity. To account for finite bandwidths, the radiometric calibration algorithm uses band-averaged spectral radiances for each band, based on the equation

$$L_X = \frac{\int_{\lambda_1}^{\lambda_2} L_X(\lambda) R(\lambda)\, d\lambda}{\int_{\lambda_1}^{\lambda_2} R(\lambda)\, d\lambda}, \tag{1}$$

where L_X is the band-averaged spectral radiance for source X with units of mW cm^{-2} μm^{-1} sr^{-1}; $L_X(\lambda)$ is the spectral radiance from the source at wavelength λ, also with units of mW cm^{-2} μm^{-1} sr^{-1}; and $R(\lambda)$ is the relative response of the band at wavelength λ. The limits of integration for (1) cover the wavelength region over which the band has a significant spectral response. The calibration values input to the radiometric calibration algorithm use band-averaged spectral radiances derived from the spectral radiance $L_X(\lambda)$ of the laboratory blackbody or the laboratory calibration sphere. Based on these values, the radiometric calibration algorithm converts the DNs produced by the instrument when viewing the Earth into band-averaged spectral radiances. For the discussions herein, the term ''radiance'' is used as a simplified form of the term ''band-averaged spectral radiance.''

The band-averaged center wavelength can be calculated also for each VIRS band using the equation

$$\lambda_X = \frac{\int_{\lambda_1}^{\lambda_2} \lambda L_X(\lambda) R(\lambda)\, d\lambda}{\int_{\lambda_1}^{\lambda_2} L_X(\lambda) R(\lambda)\, d\lambda}. \tag{2}$$

The center wavelengths for the VIRS bands are given in Table 1. For the visible and SWIR bands, the reference source spectrum $L_X(\lambda)$ is a 5900 K Planck func-

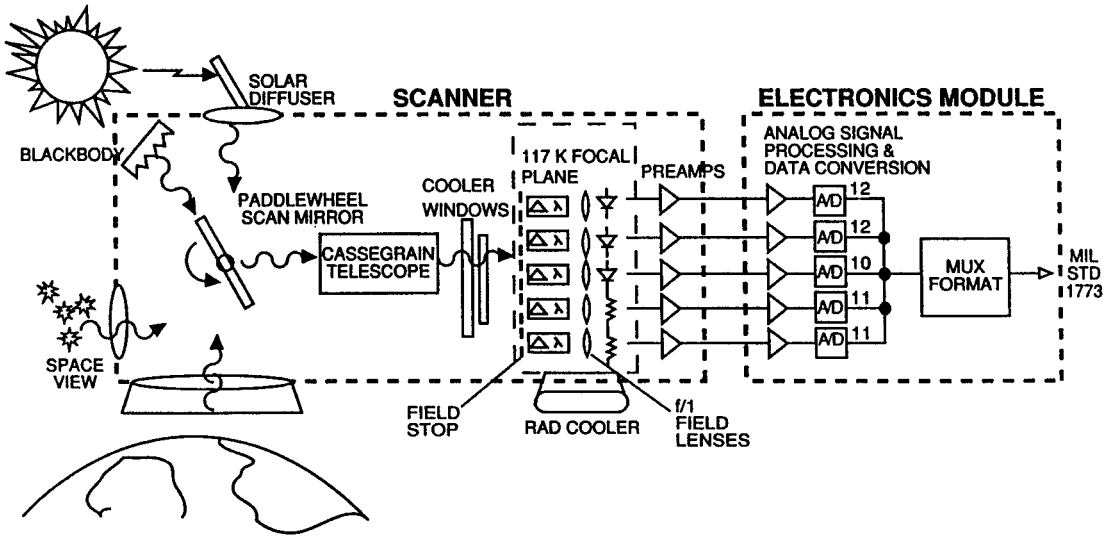

FIG. 1. A schematic of the VIRS instrument. Radiances from the Earth and the calibration targets are reflected into the telescope by the scan mirror.

tion, which approximates the spectral shape of the solar irradiance. For the thermal bands, the reference source spectrum is a 300 K Planck function, which approximates the spectral shape of the thermal radiance from the Earth. The bandwidths in Table 1 are given as the full widths at half maximum for the relative spectral responses. Additional spectral characteristics for the VIRS bands are given in Barnes et al. (1996).

a. Thermal band calibration source

For the thermal bands, the calibration radiances come from an onboard blackbody. The temperature of the blackbody's surface is measured by a set of platinum resistance thermometers. In addition, the blackbody's emissivity is determined through modeling of its surface, including its surface coating. The radiances for the calibration algorithm are stored in a lookup table derived from Planck function curves at temperatures from 260 K to 320 K at 0.5 K intervals. At each of these temperatures, there is a value of L_X for each thermal band derived from (1) using the band's relative spectral response. The radiometric calibration algorithm uses linear interpolation to derive the values of L_X for temperatures between those listed in the lookup table. The values in the table are those for an ideal blackbody radiator. For the VIRS onboard blackbody, calculation of the actual radiances also requires knowledge of its emissivity (0.985) plus a small correction for thermal emissions surrounding its surface.

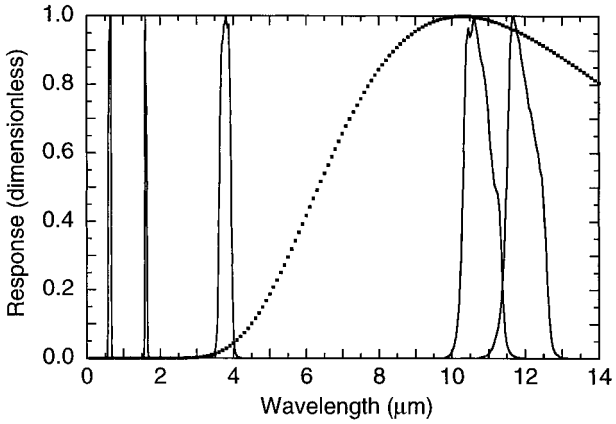

FIG. 2. The spectral response curves for the VIRS bands. For each band the response is normalized to a value of unity. The center wavelengths for the bands are listed in Table 1. The curve with symbols gives the output from a 280 K Planck function, also normalized to a maximum value of unity. A detailed plot of the spectral response of band 2, including its thermal leak, is given in Fig. 4a.

b. Visible and SWIR band calibration sources

For the visible and SWIR bands, the radiances from the laboratory calibration sphere at SBRS were used to determine the calibration coefficients before launch. For the calibration sphere, values of the spectral radiances

TABLE 1. VIRS spectral characteristics. The reference sources for the calculation of the center wavelengths are Planck function curves whose temperatures are given in the table.

Band	Band-averaged center wavelength (μm)	Reference source (K)	Bandwidth (μm)
1	0.64	5900	0.09
2	1.62	5900	0.06
3	3.80	300	0.34
4	10.75	300	1.04
5	11.94	300	1.06

TABLE 2. Radiance sources for the VIRS instrument. The VIRS telescope and detectors view the radiances from the mirror. For the discussions here, radiance is the band-averaged spectral radiance; θ represents the angles of incidence for radiances reflected from the mirror. The mirror and internal offset radiances are thermal emissions. For the space view, onboard blackbody, and diffuser, the equivalent pixel number is that for a positive incidence angle.

Radiance source	Symbol for the radiance from the source	Symbol for the radiance reflected from the mirror	Source location	Incidence angle	Equivalent pixel number
Onboard blackbody	L_{BV}	$L_{BM}(\theta_{BV})$	Internal target	−40	102
Onboard diffuser	L_{DV}	$L_{DM}(\theta_{DV})$	Internal target	−61	223
Mirror	L_M		Mirror		
Internal offset (thermal background)	L_I		Instrument housing, telescope, etc.		
Space	L_{SV}	$L_{SM}(\theta_{SV})$	Space-view port	−22.5	1
Earth	L_{EV}	$L_{EM}(\theta_{EV})$	Earth-view port	22.5 to 67.5	1 to 261
Laboratory calibration sphere	L_{CV}	$L_{CM}(\theta_{CV})$	Earth-view port	38	87
Laboratory blackbody	L_{LV}	$L_{LM}(\theta_{LV})$	Earth-view port	22.5	1

at each lamp level were determined at several wavelengths by comparison with a transfer source traceable to the National Institute of Standards and Technology (NIST). The transfer source was a quartz halogen lamp whose irradiance had been measured at a set of standard wavelengths (Walker et al. 1987). For the calibration of the laboratory sphere, the irradiance from the lamp was reflected from the surface of a diffuse reflecting placque to provide a set of spectral radiances for comparison with the output of the sphere. The comparison of the spectral radiances from the placque and the sphere was performed at the standard wavelengths using a transfer radiometer. For the calibration of VIRS, the sphere spectral radiances for wavelengths between the standard set were calculated through spline interpolation, and the band-averaged spectral radiances were calculated using (1). The uncertainty in the laboratory calibration of the VIRS visible and SWIR bands is estimated to be about 5%.

4. Thermal band equations

The VIRS algorithm accounts for three primary instrument-based effects, in addition to several second-order ones. First among the primary effects are those of the scan mirror. These are treated in terms of the radiances that are reflected from the mirror. Second are the effects of detector nonlinearity. These are treated in the determination of the calibration coefficients, which are also called the ''system gains.'' Third are the effects that come from the temperature dependence of the integrating capacitors in the VIRS electronic module. Corrections for these effects are applied to the DNs.

a. Scan mirror effects

The reflectance and the emissivity of the VIRS scan mirror are functions of the angle of incidence (AOI), θ, which is measured from the normal to the surface. Table 2 lists radiance sources for the VIRS instrument. Two of the sources—the laboratory calibration sphere and the laboratory blackbody—were used as part of the prelaunch calibration of the instrument. During the measurements the two sources were viewed through the sensor's Earth view port. For measurements on orbit, VIRS carries an onboard blackbody and an onboard diffuser. The blackbody is a continuous calibration source of thermal radiance. The diffuser, however, must be illuminated by the solar irradiance to be used. Space is used on orbit as a source with essentially no radiance, allowing measurements of the zero offsets (thermal background) of the instrument. In addition, there are two radiance sources within VIRS that are not used for calibration: the mirror and the internal offset. These two sources are central to the portion of the calibration algorithm dealing with scan mirror effects.

For an Earth scene measurement, the radiance at the detectors of the VIRS radiometer includes components from the Earth scene, the mirror, and the internal background radiance of the instrument:

$$L_{EM}(\theta_{EV}) = \rho(\theta_{EV})L_{EV} + \varepsilon(\theta_{EV})L_M + L_I, \quad (3)$$

where θ_{EV} is the incidence angle of the Earth sample on the mirror, $\rho(\theta_{EV})$ is the reflectance of the mirror for an incidence angle of θ_{EV}, and $\varepsilon(\theta_{EV})$ is the emissivity of the mirror for the same angle of incidence. The variable $L_{EM}(\theta_{EV})$ is the radiance at the detectors, L_{EV} is the Earth thermal radiance, L_M is the Planck radiance from the mirror, and L_I is the radiance from the uncooled optics, excluding the scan mirror. This internal radiance, therefore, is independent of the rotation of the scan mirror. The temperature of the optics is assumed to be constant over the time interval for each scan.

The ''zero'' value for each instrument scan is determined by a view of deep space:

$$\begin{aligned} L_{SM}(\theta_{SV}) &= \rho(\theta_{SV})L_{SV} + \varepsilon(\theta_{SV})L_M + L_I \\ &= \varepsilon(\theta_{SV})L_M + L_I, \end{aligned} \quad (4)$$

where θ_{SV} is the incidence angle of the space-view sample on the mirror, $L_{SM}(\theta_{SV})$ is the radiance at the detectors, and L_{SV} is the space-view radiance, which is assumed to be zero.

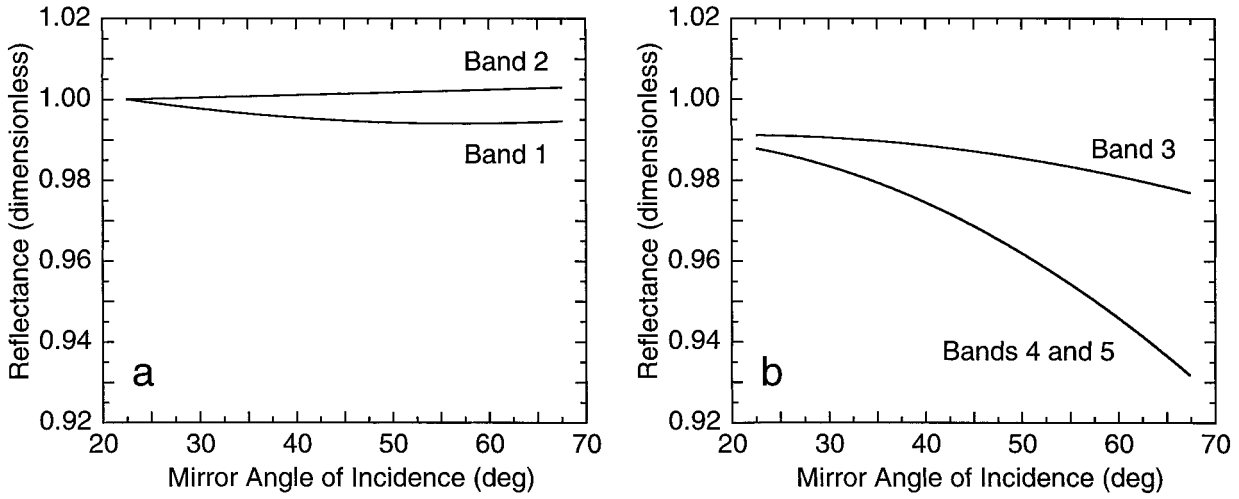

FIG. 3. Laboratory-based values for the reflectances of the VIRS scan mirror. The center wavelengths for the bands are listed in Table 1. (a) The reflectances for bands 1 and 2. (b) The reflectances for bands 3, 4, and 5. The measured reflectances for bands 4 and 5 are identical.

Earth radiances are determined from the difference of (3) and (4):

$$L_{\mathrm{EM}}(\theta_{\mathrm{EV}}) - L_{\mathrm{SM}}(\theta_{\mathrm{SV}}) = \rho(\theta_{\mathrm{EV}})L_{\mathrm{EV}} + [\varepsilon(\theta_{\mathrm{EV}}) - \varepsilon(\theta_{\mathrm{SV}})]L_M. \quad (5)$$

The solution of (5) for L_{EV} is performed by determining $[L_{\mathrm{EM}}(\theta_{\mathrm{EV}}) - L_{\mathrm{SM}}(\theta_{\mathrm{SV}})]$ using the digital numbers measured by VIRS and (11) in section 4d. The algorithm uses the Planck function radiance for the mirror L_M derived from the temperature of the mirror's scan encoder. The mirror reflectances for the range of possible incidence angles were measured before launch and stored in a lookup table. Using these values, it is possible to calculate L_{EV}.

The reflectances for the three thermal bands are shown in Fig. 3b. They come from measurements of a scan mirror witness sample (MacDonald 1997). The largest reflectances, about 0.99, are found at the start of the Earth scan, where the incidence angles on the mirror are 22.5°. The shapes of the reflectance curves with incidence angle were created by fitting the laboratory measurements to second-order polynomials. The laboratory measurements show no difference in the reflectance-versus-scan-angle curves for bands 4 and 5.

b. Deep-space measurements on orbit

It is possible to check the shapes of the reflectances curves with incidence angle using deep-space scans on orbit (Lyu et al. 2000). They are obtained by rotating the spacecraft so that the Earth-view aperture points away from the Earth's surface. For these scans, the values of the radiance from the Earth-view port—L_{EV} in (5)—are essentially zero. This gives the simplified version of that equation:

$$L_{\mathrm{EM}}(\theta_{\mathrm{EV}}) - L_{\mathrm{SM}}(\theta_{\mathrm{SV}}) = [\varepsilon(\theta_{\mathrm{EV}}) - \varepsilon(\theta_{\mathrm{SV}})]L_M. \quad (6)$$

For Earth-view pixel 1, in which θ_{EV} equals θ_{SV}, the left-hand side of (6) should equal zero. It is not possible to determine the absolute value of any emissivity or any reflectance using measurements of deep space, since (6) is based ultimately on the difference of (3) and (4). Without additional information, only the change in reflectance with scan angle is known.

c. Calibration factors

This section includes response nonlinearity effects, plus temperature effects from the electronics module. In section 4d, these factors are included in the calibration equations for the thermal bands.

1) NONLINEARITY

For the thermal bands, the responses of the HgCdTe detectors are nonlinear. If the radiance at the detector doubles, the output from the detector increases by slightly less than a factor of 2. During ground calibration, the digital numbers are fit to a quadratic function of the measured radiance:

$$\mathrm{DN}_{\mathrm{EM}} - \mathrm{DN}_{\mathrm{SM}} = q_1[L_{\mathrm{EM}}(\theta_{\mathrm{EV}}) - L_{\mathrm{SM}}(\theta_{\mathrm{SV}})] + q_2[L_{\mathrm{EM}}(\theta_{\mathrm{EV}}) - L_{\mathrm{SM}}(\theta_{\mathrm{SV}})]^2, \quad (7)$$

where q_1 is determined on a scan-line-by-scan-line basis using the onboard blackbody. This is the linear system gain, and it is different for each band and each scan line. The term q_2 in (7) cannot be determined on orbit and is obtained from the prelaunch measurements. The effect of detector nonlinearity on VIRS band 5 was treated as a quadratic correction to the linear calibration by Barnes et al. (1996). Barnes et al.'s (1996) analysis shows the magnitude of the nonlinearity to be small, causing deviations of 0.4% or less from the linear cal-

TABLE 3. Quadratic coefficients (q_2) for the VIRS thermal bands. The linear coefficients (q_1) are calculated on orbit for each scan line.

Band	q_2 (DN mW^{-2} cm^4 μm^2 sr^2)
3	−400
4	−14.0
5	−14.3

TABLE 4. Electronics module temperature correction coefficients.

Band	K_1 (K^{-1})
1	0.0012
2	0.0012
3	0.0012
4	0.0009
5	0.0009

ibration. For each of the VIRS thermal bands, the value of q_2 is negative.

For the thermal bands, the value of q_1 is derived from measurements of the onboard blackbody and the space view after each scan line:

$$q_1 = \frac{(\mathrm{DN_{BM}} - \mathrm{DN_{SM}})}{[L_{\mathrm{BM}}(\theta_{\mathrm{BV}}) - L_{\mathrm{SM}}(\theta_{\mathrm{SV}})]} - q_2[L_{\mathrm{BM}}(\theta_{\mathrm{BV}}) - L_{\mathrm{SM}}(\theta_{\mathrm{SV}})](\mathrm{DN_{BM}} - \mathrm{DN_{SM}}). \quad (8)$$

The units for q_1 are digital numbers per unit spectral radiance, DN mW^{-1} cm^2 μm sr. The value for $[L_{\mathrm{BM}}(\theta_{\mathrm{BV}}) - L_{\mathrm{SM}}(\theta_{\mathrm{SV}})]$ is calculated using (5) and the radiance from the onboard blackbody:

$$L_{\mathrm{BM}}(\theta_{\mathrm{BV}}) - L_{\mathrm{SM}}(\theta_{\mathrm{SV}}) = \rho(\theta_{\mathrm{BV}})L_{\mathrm{BV}} + [\varepsilon(\theta_{\mathrm{BV}}) - \varepsilon(\theta_{\mathrm{SV}})]L_M. \quad (9)$$

For (9), the blackbody radiance L_{BV} is calculated using the temperature of the blackbody and small corrections for its emissivity and surroundings (see section 4a). The mirror radiance L_M is calculated using its temperature and the Planck function lookup table. In the derivation presented here, the term $[L_{\mathrm{BM}}(\theta_{\mathrm{BV}}) - L_{\mathrm{SM}}(\theta_{\mathrm{SV}})]$ is treated as a single unit, although the corresponding digital numbers $\mathrm{DN_{BM}}$ and $\mathrm{DN_{SM}}$ come from two separate measurements made by the instrument.

Equations (5) and (9) are analogous except that the source radiance in (5) is that for the Earth, L_{EV}, and the source radiance in (9) is that for the onboard blackbody, L_{BV}. In (9), L_{BV} and the other terms on the right-hand side are known, allowing for the calculation of $[L_{\mathrm{BM}}(\theta_{\mathrm{BV}}) - L_{\mathrm{SM}}(\theta_{\mathrm{SV}})]$. This is the term for the blackbody and space-view radiances at the input aperture for the radiometer. Together with (8), it gives the gain term q_1. The analogy of (5) and (9) is fundamental to the operation of the VIRS calibration algorithm.

For VIRS thermal bands 4 and 5, there are two electronic gains—normal and attenuated. The attenuated gain decreases the value of $\mathrm{DN_{BM}}$, $\mathrm{DN_{SM}}$, and $\mathrm{DN_{EM}}$ by a factor of 2. This gain is a scaling factor that ensures the outputs from these bands will not saturate. The values of q_2 in (7) must be rescaled by a factor of 2 in the radiometric algorithm when the gain is changed from normal to attenuated. The linear gain q_1 rescales automatically with the gain change. The values for q_2 at the start of the VIRS mission are listed in Table 3. They are the values for the attenuated gain. After 18 months of operation there has been no need to change the gains for bands 4 and 5. The passive cooler for the focal plane continues to function very well, and the radiometric sensitivities of the bands are sufficiently high to keep the attenuated gain.

2) ELECTRONICS MODULE TEMPERATURE

For each VIRS pixel, the output from each detector is summed over the sampling period of the measurement. The sampling interval is about 280 μs. The summations are performed using integrating capacitors. There is a temperature dependence in the operation of these capacitors. Their outputs increase fractionally with temperature. The correction for this effect is given by

$$\frac{O(T_{\mathrm{REF}})}{O(T)} = \frac{1}{1 + k_1(T - T_{\mathrm{REF}})}, \quad (10)$$

where $O(T)$ is the output for temperature T, $O(T_{\mathrm{REF}})$ is the output for a reference temperature T_{REF}, and k_1 is a constant derived from preflight laboratory measurements. As shown in Table 4, the values of k_1 are small, about 0.1% K^{-1}. The right side of (10) is a multiplicative correction factor applied to the digital numbers. The value for $\mathrm{T_{REF}}$ comes from the conditions under which the laboratory measurements were made (296 K).

d. Combined calibration terms

For the thermal bands, the electronics module temperature correction from (10) is applied to (7):

$$(\mathrm{DN_{EM}} - \mathrm{DN_{SM}})\left[\frac{1}{1 + k_1(T - T_{\mathrm{REF}})}\right] = q_1[L_{\mathrm{EM}}(\theta_{\mathrm{EV}}) - L_{\mathrm{SM}}(\theta_{\mathrm{SV}})] + q_2[L_{\mathrm{EM}}(\theta_{\mathrm{EV}}) - L_{\mathrm{SM}}(\theta_{\mathrm{SV}})]^2, \quad (11)$$

which can be solved for $[L_{\mathrm{EM}}(\theta_{\mathrm{EV}}) - L_{\mathrm{SM}}(\theta_{\mathrm{SV}})]$ using the algebraic solution for quadratic functions. Therefore, it is possible to calculate L_{EV} from (5). This is the purpose of the VIRS radiometric calibration algorithm.

5. Visible and SWIR band equations

For the VIRS visible and SWIR bands, the calibration algorithm treats the same primary correction factors as found in the thermal bands.

a. Scan mirror effects

As shown in Fig. 2, an object with a temperature around 280 K—the approximate temperature of the VIRS instrument—produces negligible radiances at 0.6 and 1.6 μm. Thus, for the VIRS visible and SWIR bands, the mirror radiance (L_M) and the internal offset radiance (L_I) are effectively zero. For these bands, the radiances at the detectors during Earth scene measurements are defined by a simplified version of (3):

$$L_{\mathrm{EM}}(\theta_{\mathrm{EV}}) = \rho(\theta_{\mathrm{EV}})L_{\mathrm{EV}}. \quad (12)$$

Since the space-view radiance (L_{SV}) is also zero, (4) for the thermal bands simplifies to

$$L_{\mathrm{SM}}(\theta_{\mathrm{SV}}) = 0, \quad (13)$$

and thus, for the visible and SWIR bands, (5) simplifies to (12).

Within the VIRS radiometric calibration algorithm, the scan mirror effects for the visible and SWIR bands are handled in the same manner as those for the thermal bands except that the instrument is not a source of radiance. In the prelaunch laboratory characterization of the scan mirror, the instrument was rotated to view the output of a constant radiance source through the Earth-view aperture at several incidence angles on the mirror. The absolute value of the reflectance is not required. The reflectance is normalized to unity for an incidence angle of 22.5°—that is, for pixel 1 in each scan of the Earth. The mirror reflectances for VIRS bands 1 and 2 are shown in Fig. 3a. For the visible band, a small side-to-side difference in the reflectance of the mirror, about 0.03%, was found during the laboratory characterization of VIRS. This effect is applied in the radiometric algorithm to minimize striping in the resulting images. Mirror-side differences were not found in the SWIR or in the thermal bands.

b. Calibration factors

For bands 1 and 2, the application of the calibration factors is basically the same as for the thermal bands. The calibration equations for the visible and SWIR bands are simplified versions of their thermal counterparts.

1) NONLINEARITY

There is no evidence from the prelaunch calibration of VIRS of nonlinearity in the responses of its visible and SWIR bands. Thus, q_2 from (7) is zero, as is $L_{\mathrm{SM}}(\theta_{\mathrm{SV}})$. This is the anticipated result, based on the understanding of the characteristics of the types of detectors used for these bands (a silicon photodiode and a photovoltaic HgCdTe detector). Equation (14), which gives the relationship between digital numbers and radiance for Earth measurements, is a much simplified analog of (7):

$$\mathrm{DN}_{\mathrm{EM}} - \mathrm{DN}_{\mathrm{SM}} = q_1 L_{\mathrm{EM}}(\theta_{\mathrm{EV}}). \quad (14)$$

The determination of the radiance responsivity q_1 was determined before launch using measurements of a laboratory integrating sphere at several radiance levels:

$$q_1 = \frac{(\mathrm{DN}_{\mathrm{CM}} - \mathrm{DN}_{\mathrm{SM}})}{L_{\mathrm{CM}}(\theta_{\mathrm{CV}})}, \quad (15)$$

where $L_{\mathrm{CM}}(\theta_{\mathrm{CV}})$ is the radiance from the laboratory integration sphere reflected from the mirror.

The radiance from the mirror is calculated from the integrating sphere radiance using

$$L_{\mathrm{CM}}(\theta_{\mathrm{CV}}) = \rho(\theta_{\mathrm{CV}})L_{\mathrm{CV}}, \quad (16)$$

where L_{CV} is the radiance from the sphere during the laboratory calibration (see section 3). Although the value for $L_{\mathrm{SM}}(\theta_{\mathrm{SM}})$ is zero in (15) and (16), the value for $\mathrm{DN}_{\mathrm{SM}}$ is not, since, as with the thermal bands, bands 1 and 2 have electrical offsets to ensure that the digital numbers never go to zero.

2) ELECTRONICS MODULE TEMPERATURE

For the VIRS visible and SWIR bands, the integrating capacitors behave in the same manner as those for the thermal bands. The corrections for this effect are given by (10) and Table 4.

c. Combined calibration terms

For bands 1 and 2, the electronics module temperature corrections from (10) and Table 4 are applied to the digital numbers in (14) to give the value of the Earth radiance as reflected from the scan mirror:

$$(\mathrm{DN}_{\mathrm{EM}} - \mathrm{DN}_{\mathrm{SM}})\left[\frac{1}{1 + k_1(T - T_{\mathrm{REF}})}\right] = q_1 L_{\mathrm{EM}}(\theta_{\mathrm{EV}}). \quad (17)$$

With knowledge of $L_{\mathrm{EM}}(\theta_{\mathrm{EV}})$ from (17), it is possible to solve (12) for L_{EV}. Again, this is the purpose of the VIRS radiometric calibration algorithm.

6. SWIR band thermal leak

The relative spectral response for VIRS band 2 is shown in Fig. 4a. It is bimodal with a second response peak near 5.2 μm. The band is designed to measure the reflected solar irradiance, and the second peak is in a wavelength region in which that light source is negligibly small. Using (1)—the Planck function—and the spectral response from Fig. 4a, it is possible to calculate the band-averaged spectral radiance for band 2, in the absence of reflected solar irradiance, as a function of the temperature of the source. These are the theoretical radiances at the input aperture of the instrument for a blackbody source at a series of temperatures. They are listed in column 2 of Table 5 and are plotted in Fig. 4b. In this figure, the calculated results are fitted to a fourth-order polynomial.

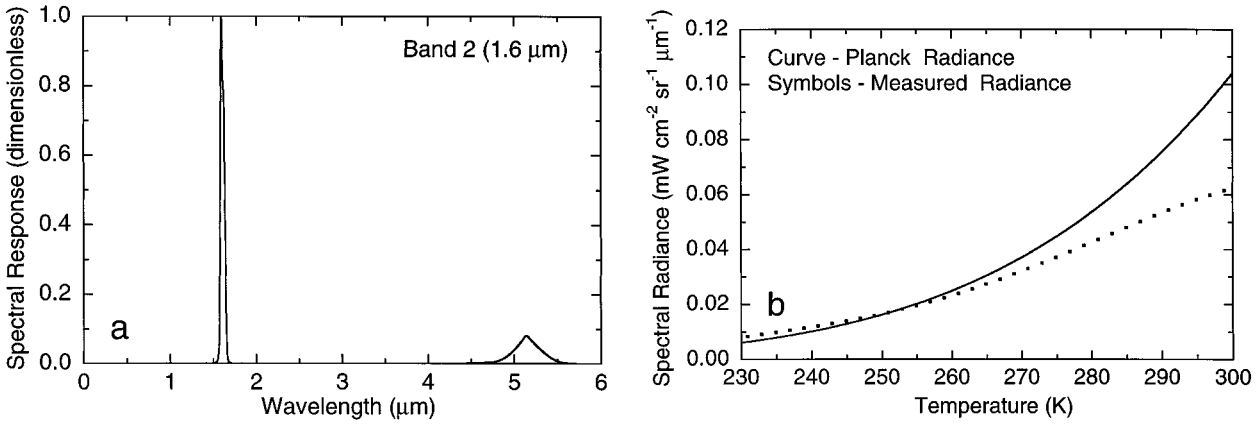

FIG. 4. Values for the VIRS band 2 red leak. (a) The relative spectral response of band 2. (b) The band-averaged spectral radiances from the red leak. The curve gives the values calculated for a blackbody source near the input aperture of the instrument. The symbols give the results of nighttime measurements over the Indian Ocean.

On 2 February 1998, a set of nighttime scans of the Indian Ocean was made using VIRS bands 1 and 2. These scans were part of an experiment to determine the radiances from the thermal leak as a function of scene temperature. The band 2 radiances from the nighttime measurements, given as a fourth-order polynomial fit, are also plotted in Fig. 4b and are listed in column 3 of Table 5. The abscissa of Fig. 4b gives the temperature for each measurement at nadir as determined by the 10.8- and 11.9-μm bands. The measurements show that the measured thermal radiances from band 2 match the calculated blackbody values in Table 5 for temperatures below 260 K. However, the measured radiances trend lower than the calculated values as the scene temperature increases. At 300 K, the radiances from the nighttime measurements are about a factor of 2 less than those calculated from the Planck function curves. This divergence is due primarily to absorption by water vapor in the atmosphere.

The results from the nighttime measurements provide a rudimentary correction for the daytime measurements from band 2. The upwelling solar-reflected radiances at 1.6 μm are independent of the thermal radiances at 5.2 μm, and vice versa. Using the VIRS thermal bands to determine the scene temperatures, the nighttime-based radiances can be calculated using Table 5 and subtracted from the daytime measurements. The measured nighttime radiances in Table 5 are incomplete, with no measurements for scene temperatures greater than 300 K. In addition, the nighttime radiances are based on a single dataset collected over the Indian Ocean. These radiances should not be considered typical of radiances found over dry landmasses, such as the Sahara Desert. Ultimately, an extended set of nighttime measurements or an external source of columnar water vapor values will be required to provide an adequate correction for the band 2 thermal leak.

TABLE 5. SWIR band thermal leak band-averaged spectral radiances versus source temperature. The Planck function spectral radiances are calculated for a blackbody source at the entrance aperture of the instrument. The measured spectral radiances come from a nighttime dataset taken over the Indian Ocean.

Blackbody temperature (K)	Planck function spectral radiance (mW cm^{-2} μm^{-1} sr^{-1})	Measured spectral radiance (mW cm^{-2} μm^{-1} sr^{-1})
320	0.1864	
310	0.1407	
300	0.1042	0.0625
290	0.0756	0.0535
280	0.0537	0.0427
270	0.0371	0.0322
260	0.0250	0.0233
250	0.0163	0.0166
240	0.0102	0.0119
230	0.0062	0.0082
220	0.0036	

The Planck function values in Table 5 assume no absorption by gases in the path between the source and the instrument. For measurements on orbit, atmospheric water vapor and other gases attenuate the upwelling radiance in the spectral region of the ''red leak.'' As shown in Fig. 5, the 4–6-μm wavelength region includes significant atmospheric absorption by water vapor. The figure gives the transmission spectrum for a water vapor amount of 3.33 g cm^{-2}, which is a typical column amount for water vapor over a tropical ocean. For this column amount, the atmosphere transmits very little of the ocean radiance for wavelengths from 5 to 6 μm. For an ocean source with a temperature of 300 K and for the values in Fig. 5, the top-of-the-atmosphere radiance is reduced to about 14% of the radiance at the surface. This calculation does not include other factors, such as absorption by gases other than water vapor, scattering by aerosols, or radiance produced by the atmosphere itself. Still, for the band 2 red leak, the transmission of radiance through the atmosphere is a very strong function of the water vapor column amount. For

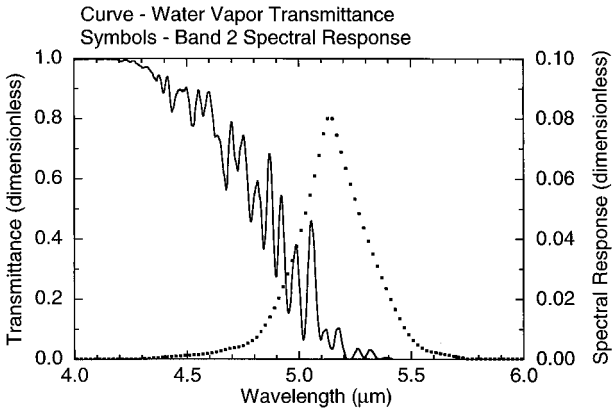

FIG. 5. Water vapor transmittance in the wavelength region of the red leak. The curve gives the atmospheric transmittance spectrum for a water vapor column amount of 3.33 g cm^{-2}. The symbols give the spectral response of band 2.

this reason, we feel that the corrections from Table 5 are good to no better than ±50%.

For most daytime scenes, the uncorrected red leak contributes about 2%–3% of the total radiance in band 2. However, for measurements in which the reflected solar irradiance is low, the effect is more substantial. The VIRS team does not anticipate adding a red leak correction to the radiometric calibration equation for the calculation of the band 2 radiances.

7. Diffuser measurements

a. Prelaunch diffuser characterization

For VIRS bands 1 and 2, the reflectance of the onboard solar diffuser was measured in the laboratory using a calibrated 1000-W quartz FEL lamp as a known source of irradiance. The digital numbers from the VIRS instrument were used to calculate radiance from the diffuser while the diffuser was illuminated by the lamp. VIRS did not view the FEL lamp directly, since the flux from the lamp did not fill the instrument's input aperture. The basic equation for the reflectance from a diffuse surface, using the notation of the VIRS radiometric calibration algorithm, is

$$B = \frac{L_{\mathrm{DV}}}{\pi E_{\mathrm{FEL}}} = \frac{L_{\mathrm{DM}}(\theta_{\mathrm{DV}})}{\rho(\theta_{\mathrm{DV}})\pi E_{\mathrm{FEL}}}, \tag{18}$$

where B is the bidirectional reflectance distribution function (BRDF) for the diffuser, with units of sr^{-1}; E_{FEL} is the irradiance from the FEL lamp, with units of mW cm^{-2} μm^{-1}; and $L_{\mathrm{DM}}(\theta_{\mathrm{DV}})$ is the diffuser radiance as reflected from the scan mirror during the diffuser characterization. Irradiance E_{FEL} was calculated using the lamp's spectral irradiance curve, the relative spectral response of the VIRS band, and (1), plus a distance correction, since the lamp was used at a distance different from that of its calibration. For the laboratory measurements of the diffuser reflectance, the radiance from the scan mirror was calculated using (17):

$$L_{\mathrm{DM}}(\theta_{\mathrm{DV}}) = \frac{(\mathrm{DN}_{\mathrm{DM}} - \mathrm{DN}_{\mathrm{SM}})\left[\dfrac{1}{1 + k_1(T - T_{\mathrm{REF}})}\right]}{q_1}, \tag{19}$$

where q_1 is the responsivity determined from measurements of the laboratory calibration sphere. The value of $L_{\mathrm{DM}}(\theta_{\mathrm{DV}})$ allows for the calculation of the BRDF of the diffuser in (18). The use of the sphere-based laboratory calibration to determine the reflectance of the diffuser has tied the value of B in (18) to the prelaunch value of q_1 in (19):

$$B = \frac{(\mathrm{DN}_{\mathrm{DM}} - \mathrm{DN}_{\mathrm{SM}})\left[\dfrac{1}{1 + k_1(T - T_{\mathrm{REF}})}\right]}{q_1\rho(\theta_{\mathrm{DV}})\pi E_{\mathrm{FEL}}} = \frac{k_2}{q_1\rho(\theta_{\mathrm{DV}})\pi E_{\mathrm{FEL}}}, \tag{20}$$

where k_2 is the value of the digital numbers from the prelaunch measurements (including the correction for the electronics module temperature). As shown in (20), the value of B is also tied to the irradiance from the standard lamp during the laboratory characterization. The value of B used here is for an irradiance ray that is normal to the input aperture of the diffuser housing. In addition, there is a two-dimensional correction to B, based on a cosine function, for irradiance rays that are not normal to the aperture.

b. Diffuser measurements on orbit

For measurements on orbit, it is possible to calculate another responsivity q_1^* using the reflectance of the solar diffuser and the irradiance from the sun. This calculation requires a model solar irradiance spectrum (Wehrli 1985) plus a correction for the difference of the Earth–Sun distance from one astronomical unit. In the following equations, this irradiance term is called E_{SUN}. For the measurements of the Sun, the radiance from the diffuser is given by a rearranged version of (18):

$$L_{\mathrm{DV}} = B\pi E_{\mathrm{SUN}}. \tag{21}$$

The radiance at the detectors requires an additional term for the reflectance of the scan mirror:

$$L_{\mathrm{DM}}(\theta_{\mathrm{DV}}) = \rho(\theta_{\mathrm{DV}})L_{\mathrm{DV}} = \rho(\theta_{\mathrm{DV}})B\pi E_{\mathrm{SUN}}. \tag{22}$$

Using $L_{\mathrm{DM}}(\theta_{\mathrm{DV}})$, (15), and the correction for the electronics module temperature, it is possible to calculate a radiance responsivity from measurements of the solar diffuser:

TABLE 6. Calibration coefficients for the visible and SWIR bands. The coefficients from the laboratory measurements (q_1) were used at launch. The coefficients from the measurements on orbit (q_1^*) were substituted for the laboratory values.

Band	q_1 (DN mW^{-1} cm^2 μm^1 sr^1)	q_1^* (DN mW^{-1} cm^2 μm^1 sr^1)	B (sr^{-1})	E_{SUN} (mW cm^{-2} μm^{-1})
1	73.98	69.30	0.286	168.16
2	474.1	433.8	0.293	24.559

$$q_1^* = \frac{(\mathrm{DN}_{DM} - \mathrm{DN}_{SM})\left[\dfrac{1}{1 + k_1(T - T_{REF})}\right]}{L_{DM}(\theta_{SV})}$$

$$= \frac{(\mathrm{DN}_{DM} - \mathrm{DN}_{SM})\left[\dfrac{1}{1 + k_1(T - T_{REF})}\right]}{\rho(\theta_{DV})\pi B E_{SUN}}$$

$$= \frac{k_3}{\rho(\theta_{DV})\pi B E_{SUN}}, \quad (23)$$

where k_3 is the value of the digital numbers from the measurements on orbit (including the correction for the electronics module temperature). The radiance responsivity from the on-orbit measurements q_1^* is not the same as the responsivity from the prelaunch measurements q_1. However, the two are related. This can be seen when the value for B from (20) is substituted into (23):

$$q_1^* = q_1\left(\frac{E_{FEL}}{k_2}\right)\left(\frac{k_3}{E_{SUN}}\right). \quad (24)$$

Ideally, the two radiance responsivities q_1 and q_1^* should be the same, with the ratio containing E_{FEL} in (24) canceling the ratio containing E_{SUN}. However, there are uncertainties in the irradiance of the FEL lamp in the laboratory measurements as well as uncertainties in the solar irradiance model used for the measurements on orbit (Wehrli 1985). In addition, there was no means of determining the changes in B from the time of the diffuser characterization in the laboratory to the time of the first diffuser measurements on orbit. As a result, it was not anticipated that the agreement between the laboratory value for q_1 would agree exactly with the initial value for q_1^* from the solar measurements.

During the first two months of on-orbit operation, a set of three solar measurements was taken. From these measurements initial values of q_1^* were determined. These values are listed in Table 6. For the visible band, the change from the laboratory value (q_1) was 6%. For the SWIR band the change was 9%. On 23 February 1998, the values for q_1^* in Table 6 were placed in the calibration lookup tables for VIRS. For both bands, the changes in the calibration coefficients are within their 10% accuracy specifications, as given in the contract for the instrument. However, the changes in the calibration coefficients are outside the 5% accuracy estimate for the laboratory calibration. These changes have brought the calibration of these bands into good agreement with the corresponding calibrations for *GOES-8/NOAA-14* (*National Oceanic and Atmospheric Administration–14*) (P. Minnis 1998, personal communication).

The diffuser is used also to measure changes in the responsivities of VIRS bands 1 and 2. Assuming that there is no change in the diffuser reflectance on orbit, the fractional changes in the diffuser measurements over time will track the fractional changes in q_1^*. VIRS carries no device to determine changes in the reflectance of the solar diffuser on orbit. However, the diffuser assembly does have a cover door that remains closed except for the periods when diffuser measurements are made. These measurements occur about twice a month, and the exposure of the diffuser during each measurement lasts a few minutes. In addition, VIRS makes measurements of the radiance from the surface of the moon several times a year. The surface of the moon is considered unchanging over the lifetime of the TRMM mission. Lunar measurements are used as a check for changes in either the VIRS responsivity or the reflectance of the onboard diffuser.

8. Estimated uncertainties

For the start of the VIRS mission, the uncertainties of the radiances from the visible and SWIR bands were calculated to be 6%. These are the uncertainties for the values of q_1^* in Table 6. The primary component of these uncertainties, about 5%, comes from the laboratory calibration of the bands. A second component comes from uncertainties in the change of the instrument from its laboratory calibration to the start of on-orbit operations. The uncertainty contribution from the mirror reflectance is believed to be small, since the reflectance corrections for these bands are 1% or less. Other instrumental uncertainties are also believed to be small.

The uncertainties for the thermal band radiances were calculated to be 3%, half those for the visible and SWIR bands. In terms of temperature, the uncertainties are about 2 K at 300 K. The uncertainty in the radiance from the onboard blackbody, combined with the uncertainty in the linearity of the response of the detectors, accounts for 2% of the total. We assume that the changes in the instrument response is negligible during the transfer of VIRS to orbit. However, there is evidence that the prelaunch characterization of the mirror reflectances for bands 4 and 5 are in error by 2%. As shown in Fig. 3, the prelaunch reflectances for these bands are the same. From measurements on-orbit (Lyu et al. 2000), the reflectances for bands 4 and 5 differ by up to 2%. However, the use of the on-orbit reflectances does not remove the mirror as a primary source of uncertainty for the VIRS thermal radiances.

9. Concluding remarks

The VIRS radiometric calibration algorithm converts the digital numbers for Earth scenes downlinked from the instrument on orbit into band-averaged spectral radiances. The algorithm treats the visible, SWIR, and thermal bands in the same manner. However, the effects of the scan mirror on the visible and SWIR bands are simplified by the fact that the mirror is not a source of emitted radiance for these bands. Also, the digital number to radiance conversion equations for the visible and SWIR bands are simplified versions of those for the thermal bands, since their detectors do not share the nonlinear response of the thermal detectors.

The reflectance of the VIRS scan mirror for the thermal bands was determined before launch using measurements of a witness sample—that is, of a mirror that is very similar to the one in the instrument. VIRS has the capability of determining the reflectance of the mirror for the thermal bands in flight by viewing scans of deep space. The results of these on-orbit measurements are given in a companion paper (Lyu et al. 2000). They differ from the laboratory measurements by up to 2%.

VIRS carries an onboard blackbody to provide a calibration radiance for the thermal bands on each rotation of the scan mirror. For the visible and SWIR bands, there is no onboard reference radiance source. However, VIRS has the capability of viewing the Moon through the space-view port, and the Sun with the onboard diffuser. These measurements are used to monitor changes in the radiometric responsivities of the visible and SWIR bands. The results of the solar measurements on orbit are also given in a companion paper (Lyu et al. 2000).

REFERENCES

Barnes, W. L., R. A. Barnes, and A. W. Holmes, 1996: Characterization and calibration results from the Visible and Infrared Scanner (VIRS) for the Tropical Rainfall Measuring Mission (TRMM). *SPIE,* **2957,** 266–276.

——, T. S. Pagano, and V. Salomonson, 1998: Prelaunch characteristics of the Moderate Resolution Imaging Spectroradiometer (MODIS) on *EOS-AM1*. *IEEE Trans. Geosci. Remote Sens.,* **36,** 1088–1100.

Cracknell, A. P., 1997: *The Advanced Very High Resolution Radiometer (AVHRR).* Taylor and Francis, 534 pp.

Guenther, B., and Coauthors, 1998: Prelaunch algorithm and data format for the level 1 calibration products for the *EOS-AM1* Moderate Resolution Imaging Spectroradiometer (MODIS). *IEEE Trans. Geosci. Remote Sens.,* **36,** 1142–1151.

Kummerow, C., W. Barnes, T. Kozu, J. Shiue, and J. Simpson, 1998: The Tropical Rainfall Measuring System (TRMM) sensor package. *J. Atmos. Oceanic Technol.,* **15,** 809–817.

Lyu, C.-H., W. L. Barnes, and R. A. Barnes, 2000: First results from the on-orbit calibrations of the Visible and Infrared Scanner for the Tropical Rainfall Measuring Mission. *J. Atmos. Oceanic Technol.,* **17,** 385–394.

MacDonald, M. E., 1997: Testing of mirror as a function of wavelength and polarization at varying angles of incidence. Massachusetts Institute of Technology/Lincoln Laboratory Report to the Modis Project, Sept. 26, 1997.

Pease, C. B., 1991: *Satellite Imaging Instruments.* Ellis Horwood, 336 pp.

Simpson, J., R. F. Adler, and G. R. North, 1988: A proposed Tropical Rainfall Measuring Mission (TRMM) satellite. *Bull. Amer. Meteor. Soc.,* **69,** 278–295.

Walker, J. H., R. D. Saunders, J. K. Jackson, and D. A. McSparron, 1987: Spectral Irradiance Calibrations. NBS Special Publication SP-250/50, 102 pp. [Available from National Institute of Standards and Technology, Gaithersburg, MD 20899.]

Wehrli, C., 1985: Extraterrestrial solar spectrum. PMOD/WRC Publication 615, 26 pp. [Available from Physikalisch-Meterologisches Observatorium Davos and World Radiation Center, Dorfstrasse 33, CH-7260, Davos-Dorf, Switzerland.]

Weinreb, M., M. Jamieson, N. Fulton, Y. Chen, J. X. Johnson, J. Bremer, C. Smith, and J. Baucom, 1997: Operational calibration of Geostationary Operational Environmental Satellite-8 and -9 imagers and sounders. *Appl. Opt.,* **36,** 6895–6904.